PHYSICAL REVIEW A VOLUME 17, NUMBER 1 JANUARY 1978

Energy distributions of secondary electrons. III. Projectile energy dependence for ionization of He, Ne, and Ar by protons*

L. H. Toburen
Battelle Northwest Laboratory, Richland, Washington 99352

Steven T. Manson
Department of Physics, Georgia State University, Atlanta, Georgia 30303

Yong-Ki Kim
Argonne National Laboratory, Argonne, Illinois 60439

(Received 27 June 1977)

A theoretical analysis of secondary electron spectra, which has previously been applied to electron-impact ionization of atoms and molecules, is applied to the experimental data on ionization of He, Ne, and Ar by protons in the 0.1–1.5-MeV energy range. The data are also compared with *ab initio* Born-approximation calculations. Our theoretical analysis clearly brings out expected features in the secondary-electron spectra for incident proton energies of 1 MeV and up. Inner-shell contributions and the charge transfer to the continuum process tend to obscure the appearance of a simple asymptotic behavior at lower proton energies; for a given incident energy, the analysis is simpler for atoms and molecules with lower nuclear charge.

I. INTRODUCTION

The study of energy deposition by energetic charged particles in matter relies on an accurate knowledge of the energy distribution of secondary electrons ejected in ionizing collisions; i.e., the number of electrons of definite kinetic energy ejected from an atom or molecule. For fast charged particles, i.e., those with velocities several times that of the bound electrons in the outer shell of the target atom or molecule, these ionizing collisions account for 75% or more of the energy loss by the penetrating particle. Knowledge of secondary-electron distributions not only provides necessary information to understand energy deposition, but provides the detail required, when coupled with theoretical analysis, to give insight into the ionization mechanisms themselves. Data are now available for secondary electrons produced by both protons[1-11] and electrons[12-17] from a number of target atoms and molecules. The data, although becoming more numerous, are still far from complete and in some instances comparisons of results from different laboratories result in unexplained disparities.

In papers I and II of this series,[18,19] a theoretical model was presented for testing the consistency of experimental data and for extrapolating existing data to regions where measurements were unavailable. The chief attribute of this technique is that it does not require calculations involving wave functions of the colliding systems. The model makes use of known systematic trends expected for large and small energy transfers based on the Rutherford (or Mott, for electrons) and Bethe-Born theories, respectively. Since wave functions are not required, the model can easily be applied to complex molecules as well as to simple atoms; this is particularly useful in radiological applications. The model had been applied to electron-impact ionization of a number of target gases with success.[20-22] Although the procedure as developed should apply equally to protons or electrons at sufficiently high projectile energies, only a brief description of this technique has been given for ionization by protons.[20,22,23]

In this paper, we extend the application of the theoretical analysis of secondary-electron spectra to ionization by protons. In particular, we have considered ionization of the noble gases He, Ne, and Ar by protons of energy 0.1 to 1.5 MeV. These targets were chosen because of the availability of experimental data for both proton and electron impact. In addition, *ab initio* calculations have been performed, within the framework of the Born approximation, using realistic nonhydrogenic wave functions. These calculations, combined with the experimental data, were then used in conjuction with the theoretical analysis presented in I and II to assess the applicability of this analysis to ionization of complex targets by protons.

II. THEORY

The model for analyzing the secondary-electron spectra produced by ionization of atoms and molecules by fast-charged particles has been presented in I and II. In this section we briefly review the main ideas and apply them to incident protons.

One of the simplest theories for the energy dis-

tribution of secondary electrons is the Rutherford formula.[18] The Rutherford formula is based on the collision of a charged particle with an electron at rest. In reality, the target electron is bound, and hence the Rutherford formula is applicable when the binding energy can be neglected compared to the kinetic energy of the ejected electron. Furthermore, the incident particle velocity should far exceed that of the bound electron to approximate the free-electron collision assumed in the derivation of the formula. When both conditions are met, then we expect the collision between a proton and an atomic or molecular electron to be well described by the Rutherford formula[18]

$$\frac{d\sigma}{dE}=\frac{4\pi a_0^2}{T}\left(\frac{R}{E}\right)^2 , \tag{1}$$

where v is the proton speed, $T=\frac{1}{2}mv^2$ with m the *electron* mass (regardless of the incident particle), a_0 is the Bohr radius (0.529 Å), R is the Rydberg energy (13.6 eV), and E is the energy transferred to the ejected electron. For an unbound electron, all of E is converted into its kinetic energy, whereas for a bound electron, part of E is needed to overcome the binding energy. Thus, for secondary electrons from the ith subshell of an atom or molecule, the energy transfer E_i is the sum of the kinetic energy ϵ and the binding energy, i.e., $E_i=\epsilon+I_i$, with I_i the binding energy of the ith subshell. For secondary electrons from a given subshell then, Eq. (1) is modified to

$$\frac{d\sigma_i}{d\epsilon}=\frac{4\pi a_0^2R^2}{T}\frac{N_i}{(\epsilon+I_i)^2} , \tag{2}$$

where N_i is the number of electrons in the ith subshell.

We consider, then, the ratio of the measured cross section for a subshell, $d\sigma_i/d\epsilon$, to the Rutherford result per target electron, i.e., with N_i omitted from Eq. (2),

$$Y_i(E,T)\equiv\frac{T}{4\pi a_0^2R^2}(\epsilon+I_i)^2\frac{d\sigma_i}{d\epsilon} , \tag{3}$$

and when the Rutherford conditions are met, this function will approach N_i, the number of electrons in the subshell. For a target with more than one occupied subshell, this definition becomes

$$\sum_i Y_i(E_i,T)=\frac{T}{4\pi a_0^2R^2}\sum_i(\epsilon+I_i)^2\frac{d\sigma_i}{d\epsilon} , \tag{4}$$

with the sum being over the subshells that contribute to the cross section. Unfortunately, application of the analysis using Eq. (4) requires measurement of the secondary-electron spectrum, subshell by subshell, and such data are difficult to obtain. Thus, we define the function $Y(E,T)$ as

$$Y(E,T)=\frac{T}{4\pi a_0^2R^2}(\epsilon+I_1)^2\sum_i\frac{d\sigma_i}{d\epsilon}$$

$$=\frac{T}{4\pi a_0^2R^2}(\epsilon+I_1)^2\frac{d\sigma}{d\epsilon} , \tag{5}$$

where I_1 is the valence ionization potential and $E=\epsilon+I_1$. This is based on the fact that at the incident energies which we are considering, the valence electrons provide most of the contribution to the cross section.

For large energy transfer, then,

$$\sum_i Y_i(E,T)\simeq\sum_i N_i=N , \tag{6}$$

N being the number of target electrons contributing to the secondary-electron spectrum and entirely independent of ϵ. For moderate energy transfer, however, use of Eq. (5) leads to

$$Y(E,T)\simeq Y(\epsilon,T)=\sum_i\frac{(\epsilon+I_1)^2}{(\epsilon+I_i)^2}N_i$$

$$=N_1+\sum_{i\neq1}\frac{(\epsilon+I_1)^2}{(\epsilon+I_i)^2}N_i , \tag{7}$$

which depends on ϵ. This function, $Y(E,T)$, will nevertheless be seen to be quite useful.

For collisions involving small energy transfers, i.e., small ϵ, and for sufficiently fast protons, the Bethe-Born approximation should be applicable,[18] i.e.,

$$\frac{d\sigma_i}{d\epsilon}=\frac{4\pi a_0^2}{T}\left(\frac{R^2}{(\epsilon+I_i)}\frac{df_i}{d\epsilon}\ln\frac{4T}{R}+B_i(\epsilon)\right) , \tag{8}$$

where $df_i/d\epsilon$ is the optical oscillator strength density in the continuum (proportional to the photoionization cross section) and $B_i(\epsilon)$, which includes the Rutherford term, depends on the target electrons only. For high enough proton velocity (large T), the first term in Eq. (8) dominates and $d\sigma_i/d\epsilon$ exhibits the characteristics of the optical (photoionization) cross section. When the Born approximation is valid, we get, from Eqs. (5) and (8),

$$Y(E,T)=\left(\sum_i\frac{(\epsilon+I_1)^2}{(\epsilon+I_i)}\frac{df_i}{d\epsilon}\right)\ln\frac{4T}{R}$$

$$+\sum_i\frac{(\epsilon+I_1)^2}{R^2}B_i(\epsilon) . \tag{9}$$

Thus, plotting $Y(E,T)$ vs E will give optical information at low E and information on the number of target electrons involved in ionization at high E. For a target with a single subshell such as He or H_2, this information is unambiguous. However, for targets with many subshells, some interpretation will be necessary.

In order to facilitate interpretation, *ab initio* calculations, within the framework of Born approxi-

mation, have been performed for He, Ne, and Ar. The calculations used Hartree-Slater (HS) wave functions and the details are given elsewhere[10] where the He results are presented. In addition, since the importance of the optical cross section is evident, the $3p$-ϵd transition in Ar was treated using Hartree-Fock (HF) wave functions for both initial discrete *and* final continuum states; the HS results are known to be unreliable for that channel.[24] Another difficulty is encountered in calculating the Born cross section for large E: the necessity to include a large number of partial waves with high angular momenta. Equations (6) and (7) avoid this difficulty. In fact, the determination of $Y(E, T)$ for large E is almost trivial as compared to any theoretical method that uses partial waves.

An additional complication in the analysis of secondary-electron spectra resulting from proton (as compared to electron) impact ionization is the existence of an alternate mechanism for the production of secondary electrons; the charge-transfer-to-the-continuum process[1,2,10] (referred to as the continuum charge transfer hereafter). In this process, the incident proton picks up an electron from the target and forms a hydrogen atom *with the electron in a continuum state*. Since the electron is not in a bound (discrete) level, it is detected as a secondary electron traveling with the proton in the laboratory frame. The maximum contribution to the continuum charge transfer comes at threshold in the frame moving with the proton, i.e., for secondary electrons whose velocity v_e nearly matches that of the incident proton, v_p. Detailed discussion of this process is given in Ref. 1. The cross section for continuum charge transfer is known to maximize for incident proton energies in the range of 0.1 to 0.3 MeV, and decrease much more rapidly than direct ionization for higher energies.[10,20,25] In He, for example, for protons of 0.1 and 0.3 MeV, the continuum charge transfer contributes nearly half of $d\sigma/d\epsilon$ at the matching velocity. This is down to about 10%, however, for 1.0-MeV protons.[10] For still higher energy, then, this effect will be negligible on $d\sigma/d\epsilon$ and, thus, on $Y(E, T)$.

III. EXPERIMENTAL TECHNIQUE

Absolute cross sections differential in ejected electron energy and emission angle were measured for 0.3-, 1.0-, and 1.5-MeV protons on helium, neon, and argon. Measurements of electron-energy spectra at 11 angles from 15° to 125° were integrated with respect to emission angle to provide the single differential cross sections described in this paper.[26] The absolute cross sections were obtained by electrostatic analysis for the ejected-electron energy range 20 to 6 keV, where absolute values were obtained directly from experimental parameters. The low-energy portion of the electron spectra (0.5 to 200 eV) was obtained by a time-of-flight measurement which was normalized to the electrostatic results in the region of overlap. The technique used to obtain absolute cross sections based on electrostatic analysis of ejected electrons was described in detail previously[5-9] as was the time-of-flight system[27] and they will not be described here. Commercially available research grade gases were used and target densities were determined from capacitance manometer measurements of target pressure. Using the complimentary techniques of electrostatic and time-of-flight energy analysis, the measured cross sections are expected to be accurate to ±20% for ejected-electron energies above 0.5 eV. The accuracy at higher energies decreases only when the cross sections decrease to where the signal-to-background ratio becomes quite small and statistical uncertainties dominate. This region can be recognized by the scatter in the data points at the extreme high-energy end of each spectra. *Relative* cross sections reported in this work should have associated uncertaintites less than ±10% except where the statistical uncertainties are large as discussed above.

IV. RESULTS AND DISCUSSION

A. Helium

The single differential cross sections $\sigma(\epsilon)$ for ionization of helium by protons are shown in Fig. 1 where they are plotted as the ratio of measured cross section to Rutherford cross section per electron, $Y(E, T)$, vs E/R. The ratio $Y(E, T)$ was evaluated using Eq. (5) and the binding energy given by Moore,[28] $I_1 = 24.58$ eV. Since there are two electrons in helium, one would expect $Y(E, T)$ to approach the Rutherford limit of 2 for large energy loss [see Eq. (7)]; the dashed line in Fig. 1 represents this expected value. For the higher proton energies, the ratio reaches a flat plateau having a value near the expected results. The ratio is approximately 10% larger than that expected from the Rutherford theory. However, this is well within the ±20% uncertainty assigned to the *absolute* values of the measured differential cross sections. For low proton energies, the Rutherford cross section is of little use in estimating the reliability of experimental data. This is because, as discussed in Sec. II, the incident particle must have a significantly larger velocity than the atomic electrons for the Rutherford formula to be valid. For He, the bound electrons have average kinetic energy of 39.5 eV and a proton of equal velocity, as the bound electrons would have to have an energy of

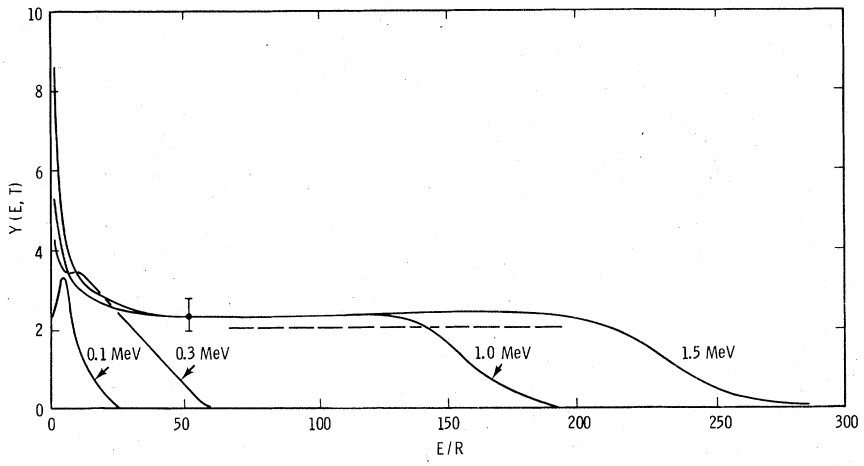

FIG. 1. Ionization of helium by protons. The ordinate $Y(E,T)$ is the ratio of the measured cross section to the Rutherford cross section [Eq. (5)]. The energy transfer E is computed as the sum of the ejected-electron energy and the valence ionization potential. According to the Rutherford theory, $Y(E,T)$ for large E should approach the number of target electrons participating in the ionizing collision. The dashed line represents the asymptotic value of two electrons. The error bar shown is representative of the 10% uncertainty in the shape of the measured cross sections. The 0.1 MeV data are from the work of Crooks and Rudd (Ref. 3).

about 73 keV. Thus, it is quite reasonable that the 0.1- and 0.3-MeV data show no Rutherford plateau, whereas the 1- and 1.5-MeV data do.

For small values of energy loss and high-energy protons, the ratios exhibit a monotonic increase as the energy loss decreases. For low proton energies, the importance of the continuum charge transfer is observed as either a contribution superimposed on the otherwise smooth distribution as is observed for 0.3-MeV protons or as a major contribution causing the entire distribution to peak above threshold as is illustrated for the 0.1-MeV data. The 0.1-MeV data are taken from the work of Crooks and Rudd.[3] The relative contribution of the continuum charge transfer is illustrated better in Fig. 2 where the low-energy portion of the spec-

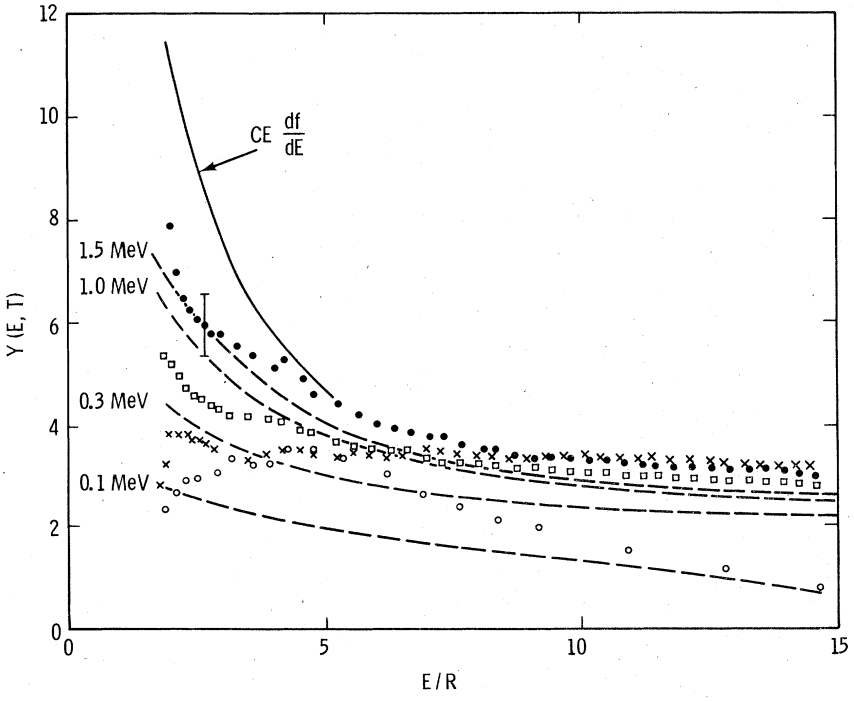

FIG. 2. Ionization of helium by protons. The dashed lines are the Born calculations from Herman-Skillman wave functions. The optical values are from Samson (Ref. 29) scaled by an arbitrary constant C. The 0.1 MeV proton data are from the work of Crooks and Rudd (Ref. 3, ○). The error bar shown is representative of a 10% relatively uncertainty in the measured cross sections. The symbols ×, □, and ● represent our measurements for proton energies 0.3, 1, and 1.5 MeV, respectively.

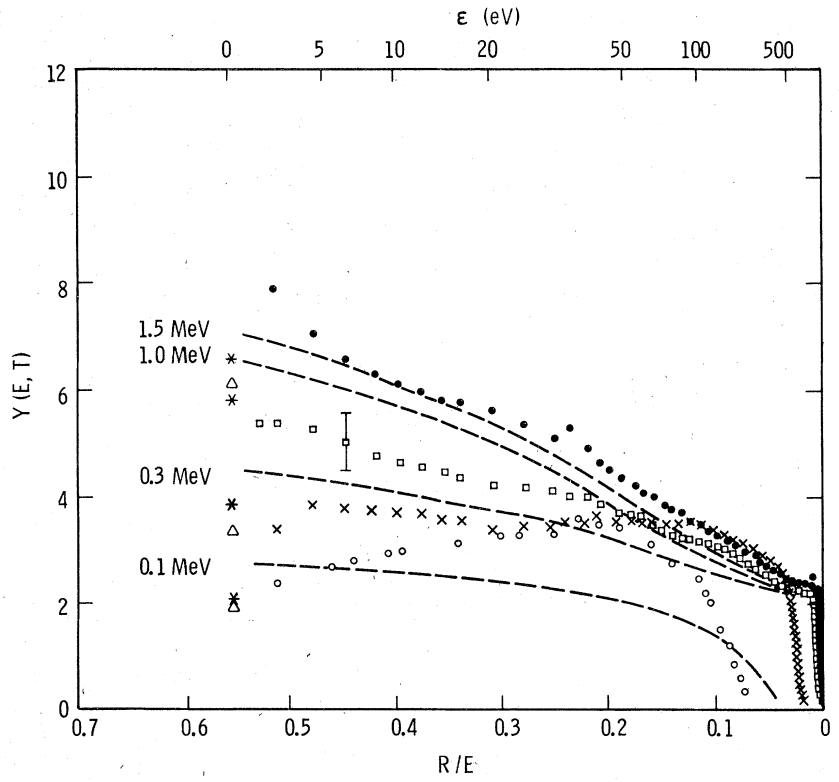

FIG. 3. Ionization of helium by protons. The dashed lines are the Born calculations from Herman-Skillman wave functions. The points for zero-energy ejected electrons are based on calculations of Kim and Inokuti (Ref. 30, *) and also on the electron-impact measurements of Grisson *et al.* (Ref. 31, Δ). The 0.1 MeV-proton data are from the work of Crooks and Rudd (Ref. 3, ○). Top scale indicates the ejected-electron energy and the error bar is representative of a 10% uncertainty in the relative values of the measured cross sections. The symbols ×, □, and ● represent our measurements for proton energies 0.3, 1, and 1.5 MeV, respectively.

tra for $Y(E, T)$ are compared with results derived from Born-differential ionization cross sections calculated from the HS wave functions; recall that the calculation does not include contributions from the continuum charge transfer. For 0.1-MeV proton impact, the values of $Y(E, T)$ derived from calculated and measured cross sections agree well at very low and high values of E/R but disagree by nearly a factor of 2 in the region of the charge-transfer peak. The disparities are also observed at higher proton energies but decrease as the proton energies increase. The maximum contribution of charge transfer for 0.3-MeV proton impact is expected at $E/R \simeq 13.5$ ($v_e \simeq v_p$) and at this value of energy loss the disparity is about 50%. For proton energies of 1.5 MeV, the differences between calculated and measured cross sections is reduced to approximately 10%.

As was discussed in Sec. II and illustrated by Eq. (9), the *shape* of the low-energy portion of the $Y(E, T)$ curves should be similar to the distribution given by $Edf/d\epsilon$ for sufficiently high-energy incident particles where $df/d\epsilon$ is the dipole oscillator strength for ionization. The comparison in Fig. 2, where the differential oscillator strength is from the compilation of Samson,[29] shows the increasing similarity between the curves representing ionization by protons and the optical values as the proton energy increases. *Note that the similarity between the proton-impact and photoionization data is on gross features only and not on magnitude.* The proton-impact data contain not only contributions from the dipole interaction (as represented by the photoionization) but also that from higher-multipole interactions. Therefore, knowledge of the photoionization cross section alone is not sufficient to estimate the proton-impact cross section.

In Fig. 3 the differential ionization cross sections presented as ratios to the Rutheford cross section are plotted against the reciprocal of the energy loss. This plot, referred to as the Platzman plot,[20] is particularly useful in that the area under each curve is proportional to the total ionization cross section. From the comparison of the 0.1- and 0.3-MeV data in Fig. 3, the importance of the continuum charge transfer in relation to total ionization is obvious for low-energy protons. Another advantage of the Platzman plot is that autoionization and Auger electrons appear as easily discernible peaks because the use of R/E as abscissa squeezes the high E portion of the spectra. The small peak at $\epsilon \sim 35$ eV in Fig. 3 represent autoionized electrons from the $2s2p^1P$ state.

Also shown in Fig. 3 are the expected values for ejection of zero-energy electrons determined both from theoretical calculations and measured for

electron-impact ionization in which the incident electron velocity was comparable to the proton velocities of our work.[30,31] The electron-impact energy range of the measurement[31] was not sufficiently large to compare to 1.5-MeV protons; however, comparisons are shown for incident electrons with velocity comparable to 0.1-, 0.3-, and 1.0-MeV protons. The calculated zero-energy values were obtained by extrapolating accurate Born cross sections for the discrete excitations according to the quantum-defect theory.[30] The agreement between the calculated values and the measured zero-energy cross sections is quite good and for the most part both are in agreement with extrapolations of the proton-impact differential ionization spectra to zero-energy ejected electrons. Certainly the agreement is well within the estimated uncertainties of ±20% in the absolute values of the measured differential ionization cross sections. The differences between the zero-energy cross sections calculated from the HS wave function and the quantum-defect theory is due to the approximate nature of the HS wave functions. One might expect the proton-impact ionization cross section to be larger than the electron-impact cross sections for the ejection of zero-energy electrons. This results from the additional interactions allowed with incident protons such as the continuum transfer and the extended range of momentum transferred to the target atom. For zero-energy ejected electrons, however, these effects appear small as agreement between theory (which does not account for the additional ionization modes) and experiment is well within experimental uncertainties.

B. Neon

The differential ionization cross sections for neon differ from the results discussed for helium in two fundamental ways. First, neon has contributions from an inner shell and, secondly, the maximum value of $Y(E, T)$ occurs considerably above the ionization threshold; if the Auger electron peak at $E/R \simeq 60$ is ignored. Figure 4 illustrates the dependence of $Y(E, T)$ on energy loss over the full spectra of ejected-electron energies for several proton energies. The 0.1-MeV data by Crooks and Rudd[3] have been included in Fig. 4 to further illustrate the behavior of $Y(E, T)$ for lower-energy protons. Since measured cross sections do not distinguish the shell from which the electron originated, $Y(E, T)$ will not add up to the total number of bound electrons until the factor $(\epsilon + I_1)^2/(\epsilon + I_i)^2$ in Eq. (7) is essentially unity. For atoms with many inner shells, such an idealized limit would be attained only at extremely high incident energy. The contribution from the K shell, whose binding energy is $\simeq 1$ keV, is still increasing in going from 1 to 1.5 MeV. For 1-MeV protons, the plateau region from approximately 70 to 90 Ry approaches a value equal to 8, which represents only $2s$ and $2p$ electrons of neon participating in the collision. From the calculation based on Eq. (7), one would expect a ratio of approximately 9 for an energy loss of 150 Ry when the K-shell contribution is included. This is in excellent agreement with the 1.5-MeV results as illustrated by the Rutherford result shown in Fig. 4. For lower-energy protons, a plateau is not established and the Rutherford formula is not applicable as was discussed earlier.

According to the Bethe-Born theory, the low-energy portion of the energy-loss spectra for ionization by sufficiently high-energy protons should be similar in shape to results derived from photoionization. This would require the peak in the spectra at low energy (i.e., low E) to be independent of proton energy (for fast protons) and to occur at the value given by optical data as indicated by Eq. (8).

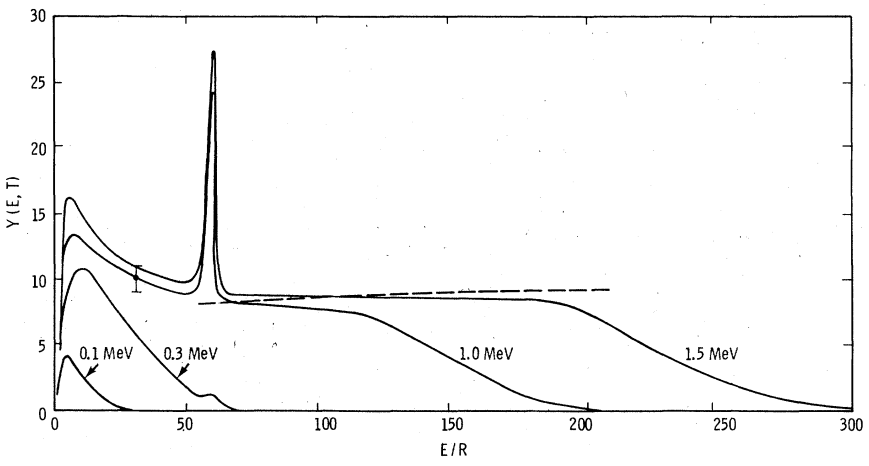

FIG. 4. Ionization of neon by protons. The dashed line represents the ratio, $Y(E,T)$, as calculated from Eq. (7). The peak at $E \simeq 60R$ represents the KLL Auger electrons and the error bar illustrates the 10% uncertainty in the relative values of the measured cross sections. The 0.1 MeV data are from the work of Crooks and Rudd (Ref. 3).

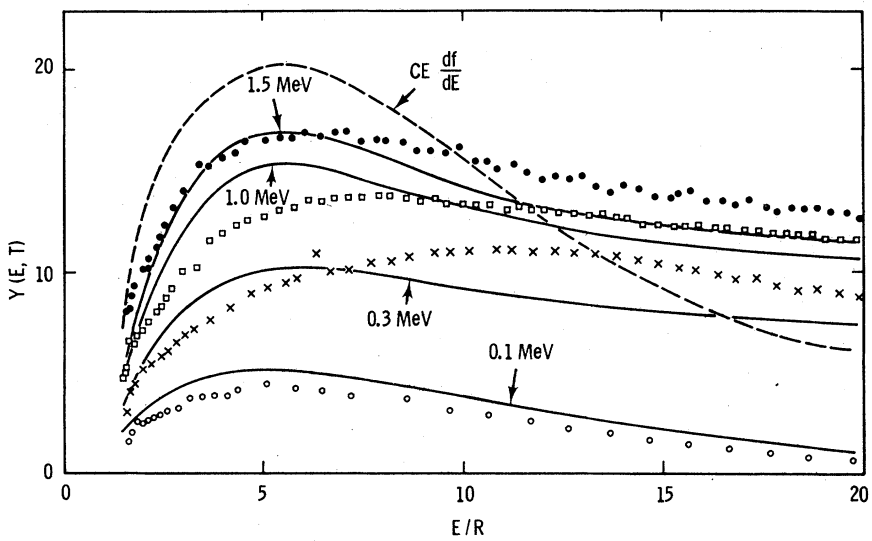

FIG. 5. Ionization of neon by protons. The solid curves represent Born cross sections and the dashed line is from the photoionization data by Samson (Ref. 29) scaled by an arbitrary constant. The 0.1 MeV data is from the work of Crooks and Rudd (Ref. 3, ○). The symbols ×, □, and ● represent our measurements for proton energies 0.3, 1, and 1.5 MeV, respectively.

It is apparent, however, from the results in Fig. 4, that the low-energy peak does not occur at a constant value of E independent of proton energy. To investigate this phenomenon further, a comparison of the measured spectra to HS-Born calculations and to optical data is shown in Fig. 5 for low E. It is interesting to note the excellent (but fortuitous) agreement between calculated and measured 0.1-MeV-proton-impact results in contrast to the disparities observed at higher proton energies. In Fig. 6, we have plotted the position of the peak in the energy-loss distribution for the proton-energy range of our work and the low-energy results of Crooks and Rudd.[3] Note that the peak position for low-energy protons is found to coincide with the energy of electrons ejected by the continuum-charge-transfer process; the Born calculation does not include contributions from continuum charge transfer. As the proton energy increases, the contribution from continuum charge transfer decreases relative to the direct ionization and moves to higher values of ejected-electron energy. In fact, from the data shown in Fig. 6, one would expect the low-energy portion of the energy-loss spectrum to be similar to the optical spectra only for proton energies of a few MeV and above.

The results for ionization of neon by protons are further illustrated in the form of a Platzman plot in Fig. 7. The importance of continuum charge transfer is particularly evident in the 0.3-MeV data

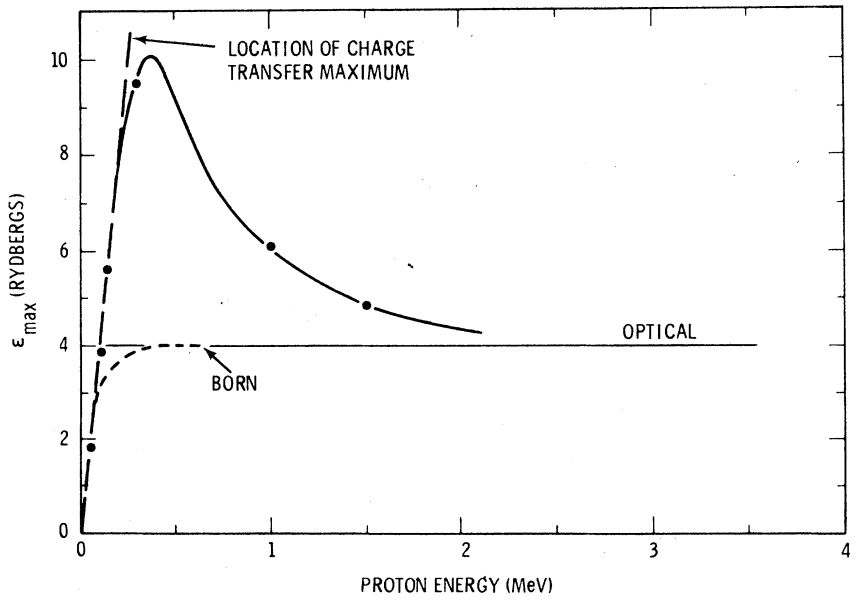

FIG. 6. Position of the low-energy maximum in the differential energy-loss spectra as plotted as a function of proton energy for ionization of neon by protons. The data for proton energies below 0.3 MeV are from the work of Crooks and Rudd (Ref. 3).

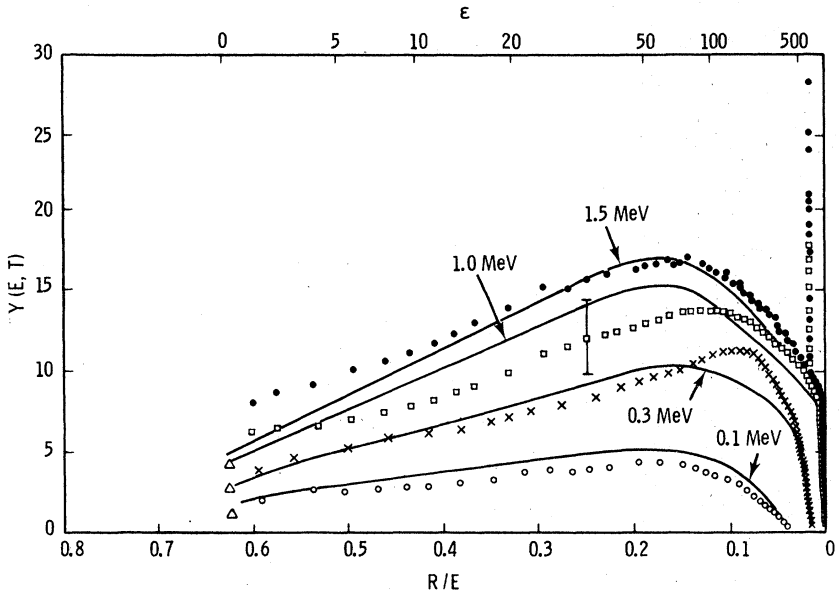

FIG. 7. Ionization of neon by protons. The solid lines represent results of the Born calculations. The points for zero-energy ejected electrons are based on the measurements of Grissom *et al.* (Ref. 31, Δ) for ionization by electrons with same velocities as the protons. The 0.1 MeV data are from Crooks and Rudd (Ref. 3, ○). The symbols ×, □, and ● represent our measurements for proton energies 0.3, 1 and 1.5 MeV, respectively.

where a sizable portion of the peak at $R/E = 0.1$ corresponds to the charge-transfer process. Agreement between measured and calculated spectra is within ±10% throughout nearly all the range of ejected-electron and proton energies; the error bar illustrated in the 1-MeV data is representative of a 10% uncertainty in relative values of the measured cross sections. The zero-energy (ejected-electron energy) points shown in Fig. 7 are those from a measurement by Grissom *et al.*[31] for electron impact. It should be noted that, within the framework of the Born approximation, the cross sections of ejection of zero-energy electrons will be nearly identical for equal-velocity electron and proton impact.[32] This is the rationale for comparing our proton data to previous results for incident electrons. For equal-velocity incident particles, the electron-impact data are in good agreement with the HS Born calculation and with the measured 0.1- and 0.3-MeV-proton results. The experimental data for 1 and 1.5-MeV protons tend toward higher values of $Y(E, T)$ compared to the Born results for zero-energy ejected electrons. The slow electrons ejected from the $2s$ and $1s$ subshells as well as those from multiple ionization are expected to increase the value of $Y(E, T)$ near $\epsilon = 0$.[21,33]

C. Argon

The ratio of measured differential ionization cross section to the Rutherford cross section for proton ionization of argon is shown in Fig. 8. The argon results differ from the neon spectra of Fig. 4 in a number of ways. The low-energy peak is very narrow, followed by a local minimum (except for 0.1-MeV data) at $E/R \simeq 4$ Ry. This rapid decline in the cross section for energy losses of approximately 2 to 4 Ry is a well-known phenomenon in photoionization.[34] This minimum is caused by the dipole matrix element going through a zero. The depth of the minimum observed for proton ionization is considerably less than that observed in photoionization because of the large number of ionization channels available to proton ionization in addition to the $3p$-ϵd dipole transition responsible for the minimum. Other prominent features of the spectra are the Auger peaks (L-MM Auger transitions) at $E/R \simeq 16$ and a broad contribution observed from approximately 10 to 50 Ry energy loss for 1 and 1.5-MeV proton impact. This latter distribution is due to contributions from the continuum charge transfer and contributions from ionization of the L shell.

Contributions from inner shells also make the evaluation of Eq. (7) difficult. If the Rutherford cross section is calculated for argon including inner-shell electrons, one must consider energy loss of several thousand Ry before the asymptotic value of 18 is reached for the ratio $Y(E, T)$. The experimental ratio does not reach the Rutherford value indicating that the inner-shell electrons are not yet fully participating in the collisions; the incident protons are not sufficiently fast for the Rutherford approximation to be valid even though the energy loss is large compared to the binding energy.

The low-energy portion of the energy-loss spectra are shown in Fig. 9 along with Born calculations and the distribution derived from optical data. Since the $3p$-ϵd transition in argon is not accurately represented by HS wave functions,[24,35] a Hartree-Fock (HF) calculation was performed for this

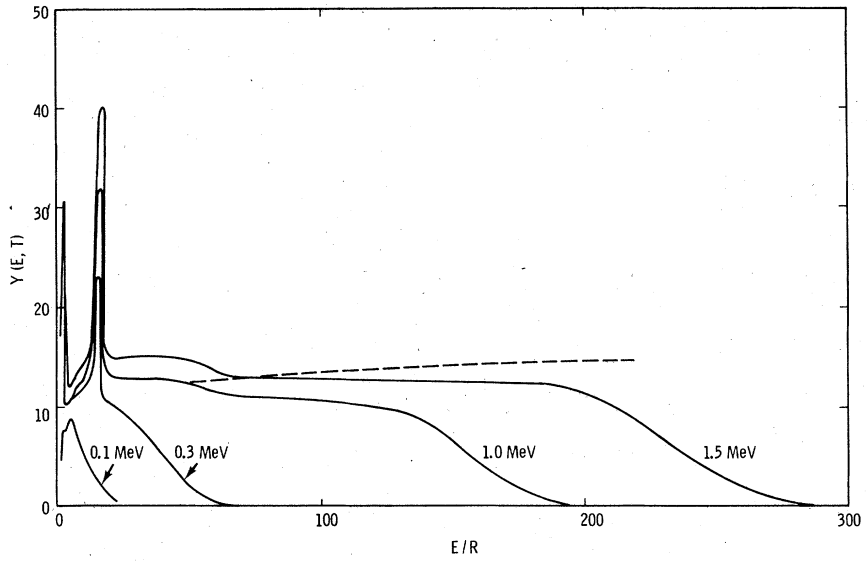

FIG. 8. Ionization of argon by protons. The 0.1 MeV data are from the work of Crooks and Rudd (Ref. 3). The dashed line represents the Rutherford value calculated from Eq. (7). The peak at $E/R \simeq 15$ is from *LMM* Auger electron emission.

channel to obtain the results shown in Fig. 9. Even with this improvement in the wave functions used in the Born calculation, the theoretical distribution peaks at somewhat higher E than either the measurement or the optical value, and the minimum is also predicted at too high an energy. For ejected-electron energies above 50 eV (4.75 Ry), measured and calculated cross sections are in excellent agreement; the exception is in the vicinity of the *L*-Auger lines ($E/R \simeq 16$) where the Auger contribution is not included in the calculation. The low-energy peak in the distributions measured for proton ionization of argon is very nearly in agreement with the position of the maximum obtained in photoionization. The actual shape and position of the low-energy peak is more readily discerned in the Platzman plot of Fig. 10 where the low-energy portion of the distribution is emphasized. In this representation, a small shift of the peak to higher E with decreasing proton energy is noted. As was shown for neon, the argon results also indicate that excellent agreement between the shape of the optical data and that of the

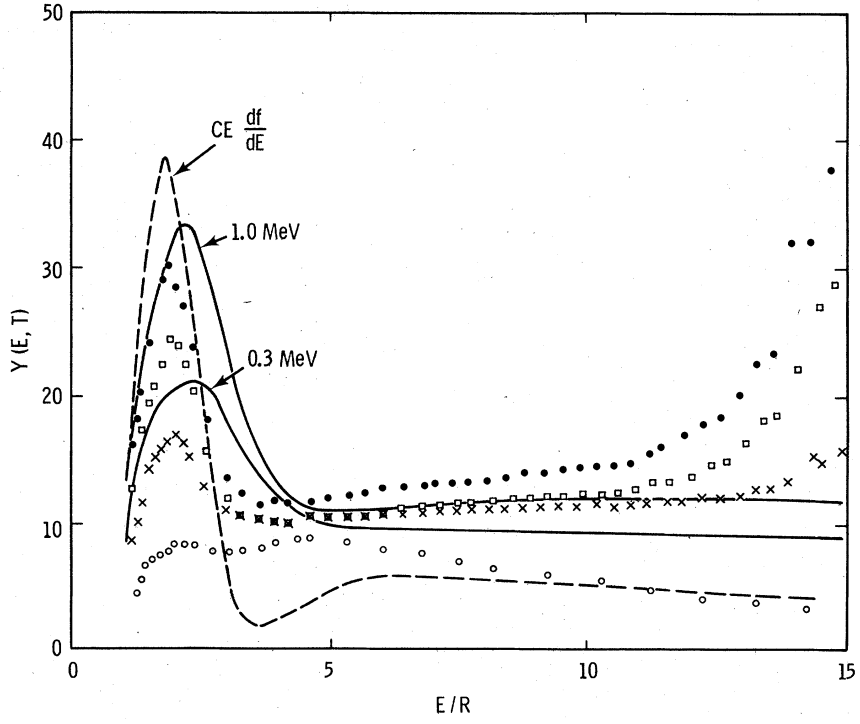

FIG. 9. Ionization of argon by protons. The solid lines represent Born calculations. The dashed curve is from the photoionization work presented by Samson (Ref. 29) scaled by an arbitrary constant C and the 0.1 MeV proton results are those of Crooks and Rudd (Ref. 3,○). The symbols ×, □, and ● represent our measurements for proton energies 0.3, 1, and 1.5 MeV, respectively.

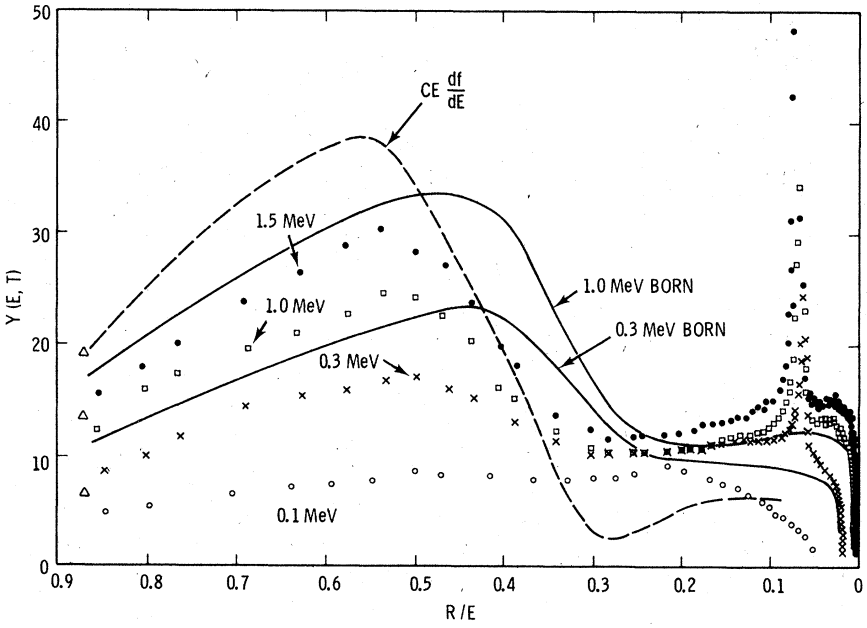

FIG. 10. Ionization of argon by protons. The measured values for zero-energy ejected electrons (Δ) are by Grissom *et al.* (Ref. 31) for incident electrons of the same speed as the protons. The scaled optical results are from Samson (Ref. 29) and the 0.1 MeV proton results are from Crooks and Rudd (Ref. 3,○). The symbols ×, □, and ● represent our measurements for proton energies 0.3, 1, and 1.5 MeV, respectively.

proton-impact data should result for proton energies greater than a few MeV. The Born calculations (solid lines in Fig. 10), although not reliable for small E, are in excellent agreement at the high-energy end of the spectra. The discrepancies between Born and measured cross section in the range $0.25 \lesssim R/E \lesssim 0.03$ $(4 \lesssim E/R \lesssim 35)$ results from continuum charge transfer and Auger-electron contributions not included in the Born calculation. If the region of the L-Auger peak is excluded, the theory and experiment agree to within approximately 10% for electron energies greater than about 50 eV ejected by 1-MeV protons.

In contrast to the agreement between the proton results and the electron-impact data for zero-energy ejected electrons observed for neon, the argon cross sections for proton impact are consistently smaller than would be expected from the zero-energy cross sections for electron impact; the electron-impact results are from Grissom *et al.*[31] Since one would expect proton results to be somewhat larger due to additional ionization channels, such as charge transfer and inner-shell ionization, this disparity for the zero-energy ejected electrons is unresolved.

D. Total cross sections

The total cross section for ionization can be obtained from the differential ionization cross section by integrating with respect to ejected-electron energy. A comparison of the total ionization cross sections for helium, neon, and argon obtained in the present work with previous proton-impact experiments is shown in Table I. These cross sections are determined primarily from the low-en-

TABLE I. Total ionization cross sections.

Target gas	Proton energy (MeV)	Cross section in 10^{-17} cm^2 [a] Present	Ref. 36	Ref. 37
Helium	0.3	5.3 ±1.0	5.14±0.31	
	1.0	1.94±0.39	2.07±0.12	2.4±0.2
	1.5	1.66±0.33	1.53±0.09	1.8±0.2
Neon	0.3	12.6 ±2.5	13.4 ±0.8	
	1.0	5.43±1.09	5.88±0.33	6.2±0.6
	1.5	4.73±0.95	4.45±0.27	4.3±0.4
Argon	0.3	30.8 ±6.1	36.7 ±2.2	
	1.0	12.3 ±2.4	15.6 ±0.9	12.8±1.3
	1.5	9.9 ±1.9	11.7 ±0.7	10.0±1.0

[a]The uncertainties shown are based on 6% and 10% errors as discussed in Refs. 36 and 37, respectively, and an estimated 20% uncertainty in the results of the present work.

ergy portion of the ejected-electron spectra; recall that the area under the curves in Figs. 3, 7, and 10 is proportional to the total ionization cross section. Since our measurements utilize a time-of-flight technique to obtain optimum accuracy in measuring the low-energy cross sections, the total ionization cross sections should possess accuracy limited only by the ± 20% uncertainty in the differential cross sections.

Our helium cross sections agree with the results of Hooper *et al.*[36] to better than 10% which is well within the combined experimental uncertainties (Hooper *et al.* estimate the uncertainty in their work at ±6%). Our result and that of Hooper *et al.*[36] both provide cross sections somewhat smaller than those by Pivovar *et al.*[37] for helium. For ionization of neon, the results of all three measurements are within about 13%, again, well within the combined uncertainties and there are no systematic differences among the reported values. The largest differences between the results shown in Table I are for argon where our present measurements are approximately 20% smaller than the results reported by Hooper *et al.*[36]; our results are in good agreement with the work of Pivovar *et al.*[37] in this case. It should be noted that the measurements of Hooper *et al.*, relied on a McLeod gauge for target-pressure determination. Mercury pumping between the cold trap isolating the target cell and the McLeod gauge has been shown to lead to errors in target-pressure measurements.[38] In the case of argon, an error in measurement as large as 20% is possible[39] and the error would contribute to an increase in the cross section derived from the measurement. In the work of Pivovar *et al.* the mercury pumping error was minimized by cooling the McLeod gauge to near 0 °C which reduced the vapor pressure of the mercury and, thus, its ability to act as a pump.[37]

V. SUMMARY

The expression of differential cross sections in terms of the ratio $Y(E, T)$ is of practical importance in assessment of experimental consistency where measurements exist and in extrapolation of existing cross sections into regions where measured values are unavailable. The use of $Y(E, T)$ depends upon the validity of asymptotic, high-energy approximations, as discussed in Sec. II: This study was undertaken to determine where these approximations are valid for *proton*-impact ionization. Previous experience with electron-impact ionization may not be entirely applicable to protons for two reasons. First is the existence of an alternate mechanism for producing secondary electrons by protons, the continuum-charge-transfer process, which can obfuscate the optical peak. Second is the fact that protons of a given velocity are far more efficient at inner-shell ionization than incident electrons of the same velocity which complicates matters since measurements are not taken subshell by subshell.

For proton energies significantly below 1 MeV, the secondary-electron spectrum produced by large energy transfer never reaches the Rutherford plateau because the incident proton is not fast enough to satisfy the conditions for Rutherford scattering. The shape of the low-energy portion of the secondary-electron distributions show little correlation to the optical data because the Bethe-Born theory is not applicable for slow incident protons. In addition, at these low proton energies, the continuum charge transfer produces a significant fraction of slow secondary electrons.

For protons in the 1–1.5-MeV range, where the continuum-charge-transfer peak has little influence, the situation is much better. A similarity in *shape* to the optical data is clearly discernible in the slow-electron region, though the slow-electron spectrum still is changing somewhat in shape as the proton energy increases. This is particularly true in the case of neon. This change of shape of the slow-electron spectrum is due to the fact that the dipole contribution is enhanced by a factor of $\ln(4T/R)$ as seen in Sec. II. On the basis of these data, it is expected that at proton energies of 4–5 MeV or higher, the slow-secondary-electron spectrum would assume the shape of the corresponding photoionization data, except for minor deviations due to inner-shell ionization.[21]

In the large energy transfer region, the behavior of $Y(E, T)$ in the 1–1.5-MeV-proton energy range is rather flat and indicative of Rutherford behavior. Note however that the height of the Rutherford plateau was independent of proton energy for helium but increased with proton energy for neon and argon. Helium has only one shell and the analysis based on $Y(E, T)$ is readily applicable. On the other hand, neon and argon have inner shells which protons of higher energies become more efficient in ionizing and thus show some dependence on the proton energy.

Examples we have presented indicate that the analysis based on $Y(E, T)$ and on corresponding optical data is particularly simple for understanding secondary-electron spectra produced by protons of 1-MeV or higher energy.

At lower proton energy, the analysis is still quite useful. Although the Rutherford plateau is no longer in evidence and the optical behavior is sometimes obscured by the charge-transfer process, the optical behavior is still discernible and contributions of the charge transfer and inner shells to

secondary-electron spectra are easily identified.

Finally, we note that while we have applied this analysis to atoms in this paper, owing to our ability to carry out *ab initio* calculations on atoms, it will apply to proton-impact ionization of molecules as well since there is nothing in the analysis which depends explicitly upon the wave function of the target; rather, it depends only upon the incident energy and inner-shell binding energies of the target.

ACKNOWLEDGMENTS

The authors would like to thank J. E. Choate and M. K. Lien for their help in operation of the accelerator and associated instrumentation. We would also like to thank M. E. Rudd for providing us with the low-energy proton results in tabular form and J. W. Hooper for helpful comments regarding details of their total ionization measurements.

---

*Work supported in part by the U. S. Energy Research and Development Administration and by the U. S. Army Research Office.

[1]M. E. Rudd and J. H. Macek, in *Case Studies in Atomic Physics* 3, edited by E. W. McDaniel and M. R. C. McDowell (North-Holland, Amsterdam, 1972), pp. 47–136.

[2]M. E. Rudd, Radiat. Res. 64, 153 (1975).

[3]J. B. Crooks and M. E. Rudd, Phys. Rev. A 3, 1628 (1971).

[4]M. E. Rudd and D. H. Madison, Phys. Rev. A 14, 128 (1976).

[5]L. H. Toburen, Phys.Rev. A 3, 216 (1971).

[6]L. H. Toburen and W. E. Wilson, Phys. Rev. A 5, 247 (1972).

[7]L. H. Toburen, Phys. Rev. A 9, 2505 (1974).

[8]W. E. Wilson and L. H. Toburen, Phys. Rev. A 11, 1303 (1975).

[9]D. J. Lynch, L. H. Toburen, and W. E. Wilson, J. Chem. Phys. 64, 2616 (1976).

[10]S. T. Manson, L. H. Toburen, D. H. Madison, and N. Stolterfoht, Phys. Rev. A 12, 60 (1975).

[11]N. Stolterfoht, Z. Phys. 248, 92 (1971).

[12]E. Ehghardt, D. H. Hesselbacher, K. Jung, and K. Willman, in *Case Studies in Atomic Physics*, edited by E. W. McDaniel and M. R. C. McDowell (North-Holland, Amsterdam, 1972), p. 159–208.

[13]E. C. Beaty, Radiat. Res. 64, 70 (1975).

[14]C. B. Opal, E. C. Beaty, and W. K. Peterson, At. Data 4, 209 (1972).

[15]N. Oda, F. Nishimura, and S. Tahira, J. Phys. Soc. Jpn. 33, 462 (1972).

[16]N. Oda, Radiat. Res. 64, 80 (1975).

[17]R. D. DuBois, thesis (University of Nebraska, 1975) (unpublished).

[18]Y.-K. Kim, Radiat. Res. 61, 21 (1975), referred to as I hereafter.

[19]Y.-K. Kim, Radiat. Res. 64, 205 (1975), referred to as II hereafter.

[20]Y.-K. Kim, Radiat. Res. 64, 96 (1975).

[21]H. C. Tickwell and Y. K. Kim, J. Chem. Phys. 64, 333 (1976).

[22]Y.-K. Kim, in *The Physics of Electronic and Atomic Collisions*, edited by J. R. Risley and R. Geballe (University of Washington, Seattle, 1976), pp. 741–755.

[23]Y.-K. Kim and T. Noguchi, Int. J. Radiat. Phys. Chem. 7, 77 (1975).

[24]S. T. Manson, Adv. Elec. Electron Phys. 41, 71 (1976).

[25]L. H. Toburen, M. Y. Nakai, and R. A. Langley, Phys. Rev. 171, 114 (1968).

[26]Double- and single-differential as well as total ionization cross sections are available in tabular form from the authors upon request.

[27]L. H. Toburen and W. E. Wilson, Rev. Sci. Instrum. 46, 851 (1975).

[28]C. E. Moore, *Atomic Energy Levels*, Nat. Bur. Std. Publ. (U.S. GPO, Washington, D. C., 1948).

[29]J. A. R. Samson, in *Advances in Atomic and Molecular Physics*, edited by D. R. Bates and I. Estermann (Academic, New York, 1966), Vol. 2, pp. 177-261.

[30]Y.-K. Kim and M. Inokuti, Phys. Rev. A 7, 1257 (1973).

[31]J. T. Grissom, R. N. Compton, and W. R. Garrett, Phys. Rev. A 6, 977 (1972).

[32]M. Inokuti, Rev. Mod. Phys. 43, 297 (1971).

[33]M. J. van der Viel and G. Wiebes, Physica 54, 411 (1970).

[34]S. J. Kennedy and S. T. Manson, Phys. Rev. A 5, 227 (1972).

[35]S. T. Manson, J. Electron Spectrosc. Relat. Phenom. 1, 413 (1972/73).

[36]J. W. Hooper, D. S. Harmer, D. W. Martin, and E. W. McDaniel, Phys. Rev. 125, 2000 (1962).

[37]L. I. Pivovar and Yu. Z. Levchenko, Zh. Eksp. Teor. Fiz. 52, 42 (1967) [Sov. Phys. — JETP 25, 27 (1967)].

[38]H. Ishii and K. Nakayama, *Transactions of the Eighth National Vacuum Symposium*, 1961 (Pergamon, Oxford, England, 1962), Vol. 1, pp. 519–524.

[39]Ch. Meinke and G. Reich, Vacuum 13, 579 (1963).